RESEARCH ARTICLE

GALAXIES

Inspiraling streams of enriched gas observed around a massive galaxy 11 billion years ago

Shiwu Zhang¹†, Zheng Cai^{1,2}*†, Dandan Xu¹, Rhythm Shimakawa^{3,4}, Fabrizio Arrigoni Battaia⁵, Jason Xavier Prochaska^{6,7}, Renyue Cen^{8,9}, Zheng Zheng¹⁰, Yunjing Wu¹, Qiong Li^{11,12}, Liming Dou¹³, Jianfeng Wu¹⁴, Ann Zabludoff¹⁵, Xiaohui Fan¹⁵, Yanli Ai¹⁶, Emmet Gabriel Golden-Marx¹, Miao Li¹⁷, Youjun Lu^{18,19}, Xiangcheng Ma²⁰, Sen Wang¹, Ran Wang¹¹, Feng Yuan²¹

Stars form in galaxies, from gas that has been accreted from the intergalactic medium. Simulations have shown that recycling of gas—the reaccretion of gas that was previously ejected from a galaxy—could sustain star formation in the early Universe. We observe the gas surrounding a massive galaxy at redshift 2.3 and detect emission lines from neutral hydrogen, helium, and ionized carbon that extend 100 kiloparsecs from the galaxy. The kinematics of this circumgalactic gas is consistent with an inspiraling stream. The carbon abundance indicates that the gas had already been enriched with elements heavier than helium, previously ejected from a galaxy. We interpret the results as evidence of gas recycling during high-redshift galaxy assembly.

imulations of galaxy formation in the early Universe indicate that low-mass galaxies grow by the direct accretion of gas from the circumgalactic medium (CGM) and intergalactic medium (IGM) (1). Both simulations and observations have shown that galaxies in low-mass dark matter halos—those with a halo mass $M_{\rm h} < 10^{12}$ solar masses (M_{\odot}) (2, 3)—can accrete streams of gas at temperatures of ~10⁴ K. These streams link the galaxy to the surrounding CGM and IGM with a filamentary web of pristine gas (gas

¹Department of Astronomy, Tsinghua University, Beijing

containing almost no elements heavier than helium) (I, 2). Transport of gas along these streams prevents it from being shock-heated while falling into the potential well of the dark matter halo, so this process is referred to as "cold-mode" accretion (2). Cold-mode accretion could explain the high star formation rate (SFR) of high-redshift galaxies and the increase in angular momentum of galaxy halos over time (4).

Although cold-mode accretion is expected for pristine gas, predictions differ for metalenriched gas (gas with higher abundances of elements heavier than helium, referred to as its metallicity). Cosmological simulations predict potentially observable quantities of metalenriched CGM around galaxies with M_h > $10^{12} M_{\odot}$ (5, 6). Because metal-enriched CGM gas can cool more efficiently than pristine gas, metal-enriched accretion (recycled inflow) could provide additional gas and boost the SFR of galaxies in massive halos $(M_h > 10^{12} M_{\odot})$ at redshift z > 2 (7-10). Observations of absorption lines toward background sources have implied the presence of metal-enriched CGM around galaxies (11), but these only provide information at a single point. To determine the spatial distribution of CGM gas requires studying its emission lines.

100084, China. ²School of Mathematics and Physics, Qinghai University, Xining 810016, China. ³National Astronomical Observatory of Japan, National Institutes of Natural Sciences, Tokyo 181-8588, Japan. ⁴Waseda Institute for Advanced Study, Waseda University, Tokyo 169-0051, Japan. ⁵Max-Planck-Institut für Astrophysik, D-85748 Garching bei München, Germany. ⁶Department of Astronomy and Astrophysics, University of California, Santa Cruz, CA 95064. USA. 7Kavli Institute for the Physics and Mathematics of the Universe, The University of Tokyo, Kashiwa 277-8583, Japan. ⁸Department of Physics, Zhejiang University, Hangzhou 310027, China. 9Department of Astrophysical Sciences, Princeton University, Princeton, NJ 08544, USA. ¹⁰Department of Physics and Astronomy, University of Utah, Salt Lake City, UT 84112, USA. 11 Kavli Institute for Astronomy and Astrophysics, Peking University, Beijing 100871, China. ¹² Jodrell Bank Centre for Astrophysics, University of Manchester, Manchester M13 9PL, UK. 13 Department of Astronomy, Guangzhou University, Guangzhou 510006, China. ¹⁴Department of Astronomy, Xiamen University, Xiamen 361005, China. ¹⁵Steward Observatory, University of Arizona, Tucson, AZ 85721, USA. ¹⁶College of Engineering Physics, Shenzhen Technology University, Shenzhen 518118, China. ¹⁷Center for Computational Astrophysics, Flatiron Institute, New York, NY 10010, USA. 18 National Astronomical Observatories, Chinese Academy of Sciences, Beijing 100101, China. 19School of Astronomy and Space Sciences, University of Chinese Academy of Sciences, Beijing 100049, China. ²⁰Department of Astronomy and Theoretical Astrophysics Center, University of California Berkeley, Berkeley, CA, 94720, USA. ²¹Shanghai Astronomical Observatory, Chinese Academy of Sciences, Shanghai 200030, China. *Corresponding author. Email: zcai@mail.tsinghua.edu.cn

Observations of MAMMOTH-1

Lyman alpha (Ly α) is an emission line of neutral hydrogen that has a rest-frame wavelength of 1216 Å. Observations of enormous Ly α nebulae with wide-field integral field spectrographs could potentially determine the physical properties and kinematics of CGM at z > 2. One such Ly α nebula is the MAMMOTH-1 nebula at $z \approx 2.31$ (coordinates: right ascension $14^{\rm h}41^{\rm m}24^{\rm s}.42$, declination $+40^{\rm o}03'09''.7$, J2000

equinox), which has Ly α emission with a jected spatial extent of 442 kpc and Ly α minosity $L_{\rm Ly} = 5.1 \pm 0.1 \times 10^{44} {\rm erg \ s^{-1}}$ (12). It resides in an overdense galaxy environment (12–14).

Our team observed MAMMOTH-1 with the Keck Cosmic Web Imager (KCWI) on the 10-m Keck II telescope in imaging spectroscopy mode centered on the Lya, C IV 1548/1550 Å, and He II 1640 Å emission lines. We also performed narrowband imaging of redshifted Ha (another line of neutral hydrogen with a restframe wavelength of 6563 Å) emission using the Multi-Object InfraRed Camera and Spectrograph (MOIRCS) on the 8-m Subaru telescope. We supplement these data with archival observations at near-infrared, x-ray, and radio wavelengths (15).

We optimally extracted images from the KCWI data (Fig. 1, A to C) (13, 15). These show that the flux peaks of the emission lines Lya, C IV, and He II coincide with a quasar (at 14^h41^m24^s42, +40°03′09″7, J2000) detected in the x-ray data (fig. S1B), which we designate as MAMMOTH-1:G-2 (hereafter G-2) (15). G-2 is located inside the nebula and provides the ionizing photons that excite the gas emission lines. The Lya, C IV, and He II emission regions are asymmetrically distributed around G-2. Both He II and C IV are spatially extended, with projected scales of 88 and 108 kpc (2σ emission), respectively, and have luminosities of $L_{\rm He~{\scriptscriptstyle II}}$ = 5.48 ± 0.13 × 10⁴² erg s⁻¹ and $L_{\rm C~{\scriptscriptstyle IV}}$ = $10.50 \pm 0.16 \times 10^{42} \text{ erg s}^{-1}$, respectively. The MOIRCS narrowband imaging (Fig. 1J) shows that the Ha emission has a projected scale of 97 kpc, with a luminosity of $L_{\rm H\alpha}$ = 2.33 \pm 0.15 \times 10⁴³ erg s⁻¹. From the archival radio observations of CO ($J = 1 \rightarrow 0$, where J is the rotational quantum number) (14), we measure the redshift of G-2 to be $z = 2.3116 \pm 0.0004$ (15). The CO $(J = 1 \rightarrow 0)$ and CO $(J = 3 \rightarrow 2)$ observations (fig. S1A) (14, 16) show that the sources around G-2 we designate as G-1, G-3, G-4, G-5, and G-6 (Fig. 1) also have redshifts of $z \approx 2.31$ and thus are located within the nebula.

We used the spectral information to construct a flux-weighted Lva velocity map (Fig. 1D). This shows two regions of gas, each with gas at a similar velocity extending for ≥100 kpc, which we refer to as regions A and B. The ionizing source, G-2, is located within region A. One-dimensional (1D) spectra (Fig. 2) extracted from selected apertures (labeled in Fig. 1E) have double- or triple-peaked structures, which we fitted with models consisting of multiple Gaussians. The Ly α and He II emission spectra have similar double- or triplepeaked profiles at each location, indicating that the line profiles are attributable to the motion of the ionized gas rather than Lya radiative transfer effects (17). Using smaller apertures (fig. S2) confirms this result (15). In the large-scale CGM where no He II is detected,

†These authors contributed equally to this work

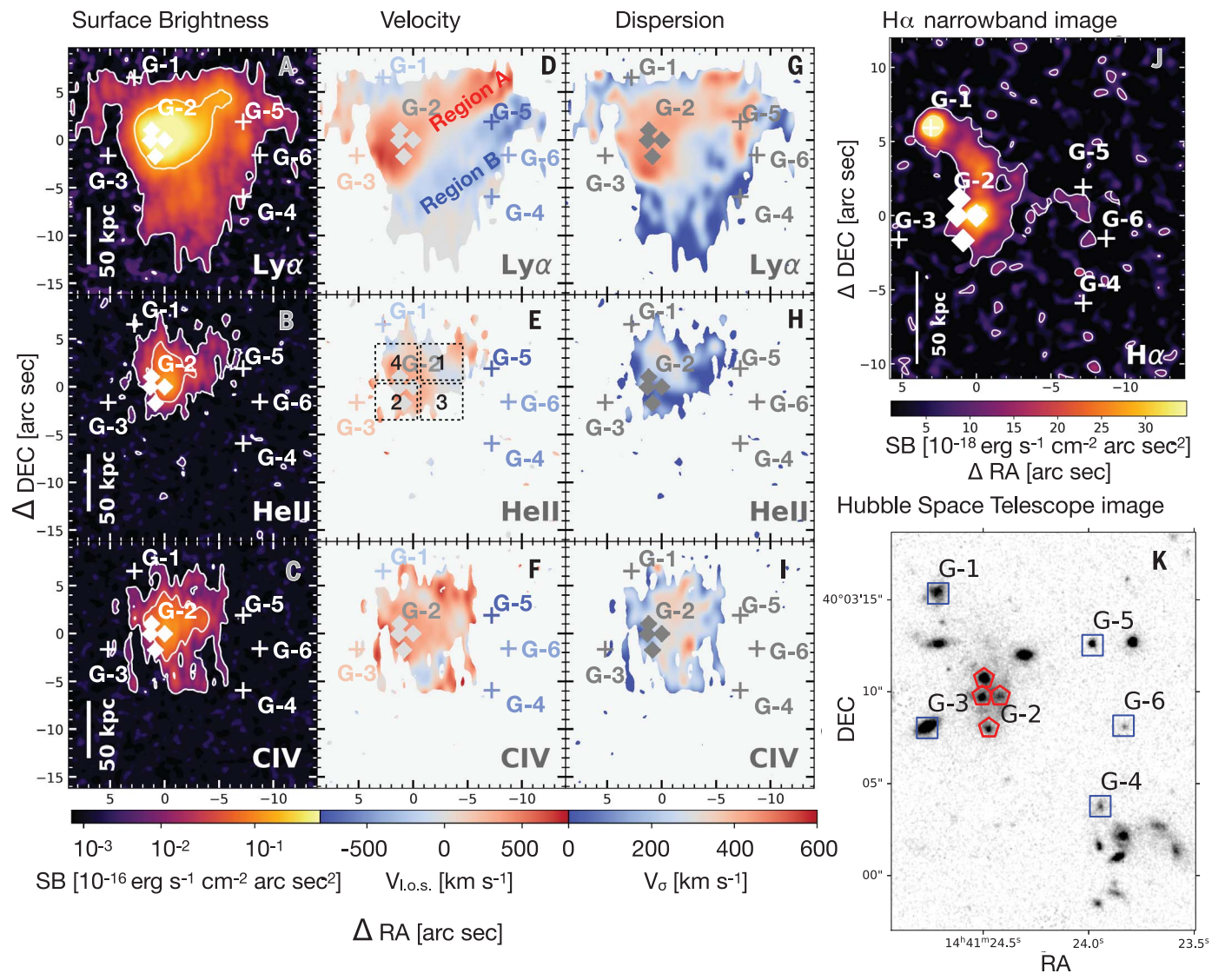


Fig. 1. Images of the extended line emission. (A to C) Optimally extracted surface brightness (SB) images of Lyα, He II, and C IV emission from the KCWI datacube. Δ RA and Δ DEC are the coordinate offsets in right ascension and declination, respectively, relative to the position of G-2 ($14^{14}41^{m}24^{s}.42$, $+40^{\circ}03'09'.7$, J2000). Cross and diamond symbols labeled G-1 to G-6 are galaxies at redshift z = 2.31, measured in both the CO ($J = 1 \rightarrow 0$) (I4) and CO ($J = 3 \rightarrow 2$) observations (I6). White contours outline regions of I60 and I61 and I62 and I63 detection of Lyα emission and regions of I63 and I63 detection for He II and C IV. In each case, the emission line extends over CGM scales. (**D** to **F**) Flux-weighted line-of-sight velocity (I610 maps.

The Ly α velocity map is labeled to indicate the large-scale red strip (region A) and blue strip (region B) (see also Fig. 4A). The four dashed squares in the He II velocity map are each 4" by 4" wide, and the extracted 1D spectra from each of the four apertures are shown in Fig. 2. (**G** to **I**) Flux-weighted velocity dispersion (ν_{σ}) maps. (**J**) H α narrowband image (seeing 0.4"). Symbols are the same as in (A) to (C). The flux peak of H α coincides with the Ly α , He II, and C IV emission. (**K**) Hubble Space Telescope image of the galaxy group, using the filter F160W, which is rest-frame optical. Four clumps within 2" of G-2 are circled in red, and galaxies at $z \approx 2.3$ are marked with blue boxes. Coordinates are J2000 equinox.

we expect radiative transfer effects to be weaker, so the Ly α also traces the cool gas kinematics in those regions (15).

Analysis of line ratios

Using the diffuse C IV, He II, and H α emission lines, we studied the properties of the CGM with spatially resolved line ratio diagnostics (15). H α emission is better suited for line ratio diagnostics than Ly α because it is less affected by resonant scattering (18). H α is also less

affected by dust attenuation; we estimate that the potential effect of dust on the line ratios is <15% (15). We consider two possible emission mechanisms: In the pure photoionization scenario, the gas is highly ionized by strong ultraviolet radiation from the quasar, causing the line emission to be dominated by recombination. In the alternative shock-with-precursor scenario, the gas moves at a velocity higher than the local sound speed, so a shock front forms at the leading edges of the clouds. Such

shocks could heat the gas to sufficiently high temperatures that it cools by emitting soft x-rays (19). Model line ratios are shown in fig. S5 for the pure photoionization scenario and in Fig. 3 for the shock-with-precursor scenario. The observed C $\mbox{\sc iv}/\mbox{\sc Ha}$ ratio is consistent with both scenarios, whereas the He $\mbox{\sc ii}/\mbox{\sc Ha}$ ratio can only be produced by the shock-with-precursor scenario—it is an order of magnitude smaller than predicted for the pure photoionization model. We examined alternative assumptions

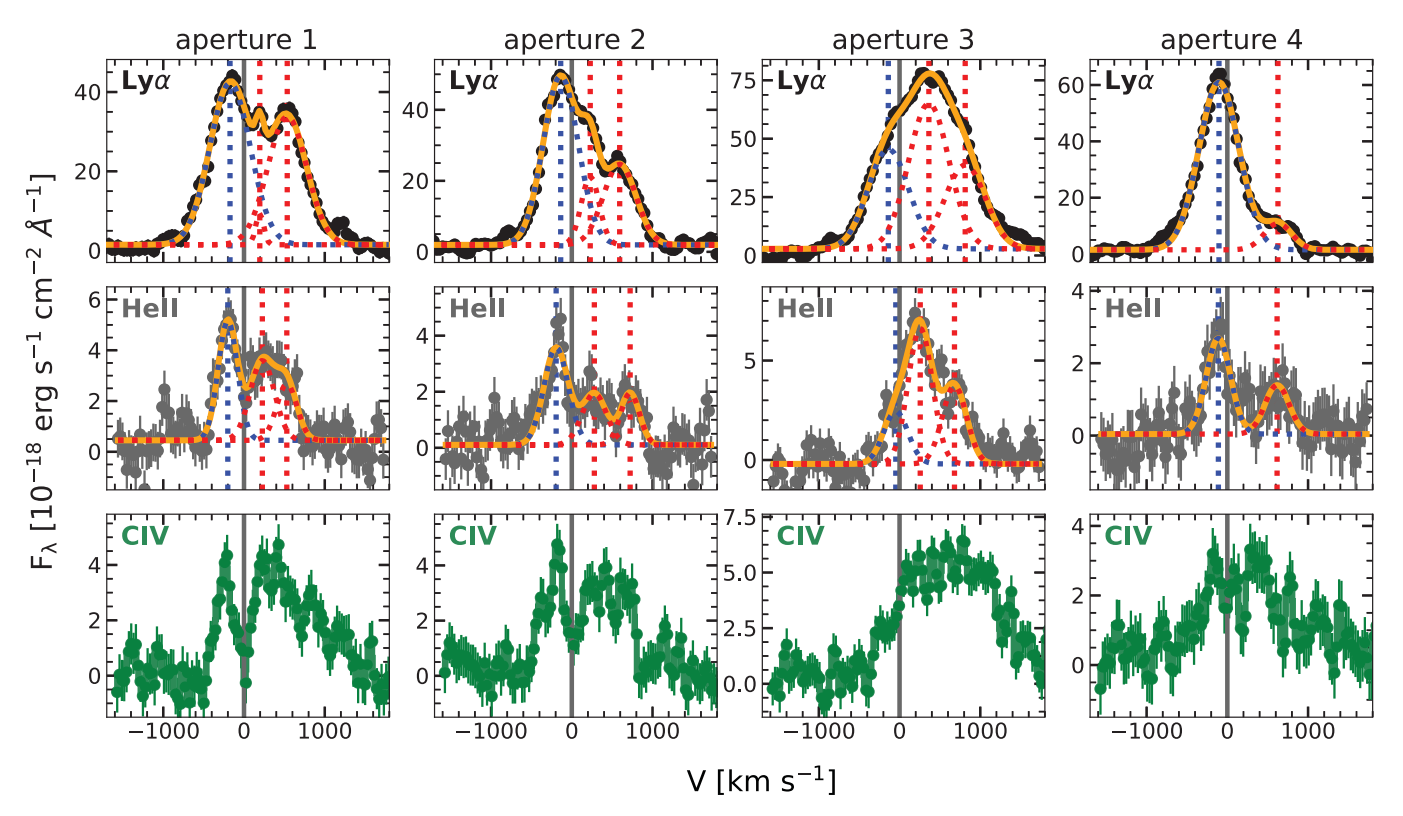
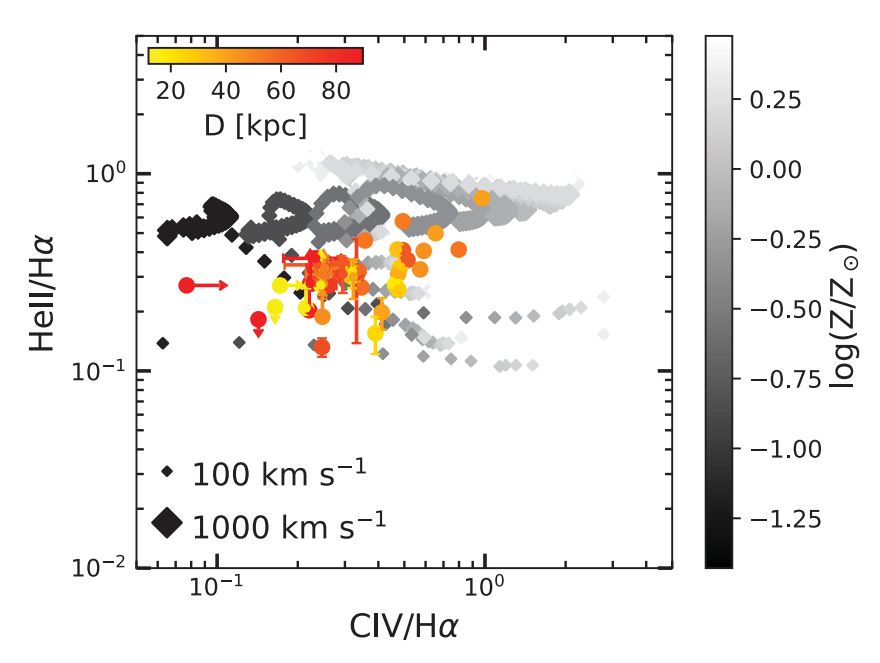


Fig. 2. One-dimensional spectra of the Ly α , He II, and C IV emission. These spectra were extracted from the apertures shown in Fig. 1E. F_{λ} is the flux density at wavelength λ . Dots (with 1σ error bars) show the observed spectra, while the orange lines are a model consisting of multiple Gaussians fitted to the data. The individual Gaussian components are shown with dashed lines. Numerical values

are listed in table S1. The vertical dashed lines mark the peaks of these Gaussian components. Each model requires two or three components to fit the data. Because He $\scriptstyle\rm II$ is a nonresonant line, the multiple components indicate gas motion of the CGM rather than resonant scattering effects (17). C $\scriptstyle\rm IV$ is a doublet, so it was not modeled with Gaussians.

Fig. 3. Line ratios He II/H α and C IV/H α for the observations and the shock-with-precursor scenario. Colored dots are the observations, and gray diamonds are predictions from the model (19). Error bars are 2σ , and arrows denote lower or upper limits. Colors indicate the projected distance (D) between the southeast aperture and each of the other apertures used to extract line emission (fig. S4). For the model, the gray scale represents metallicity (Z), and symbol sizes scale with the model shock velocity (100 to 1000 km s⁻¹ in steps of 25 km s⁻¹), as indicated in the legend. The observed line ratios of He II/H α and C IV/H α are consistent with the shock-with-precursor scenario at CGM metallicity of 0.1 to 1.0 Z_{\odot} , across a distance of ≈100 kpc.



about the quasar emission and dust attenuation, finding that a photoionization scenario is unlikely to produce the observed line ratios in all cases (15). We therefore conclude that the shock-with-precursor scenario is the mechanism responsible for the observed emission line.

From the line ratio diagnostics, we find that the CGM metallicities are within 2σ of the solar metallicity (Z_{\odot}) (Fig. 3). This is an order

of magnitude higher than previous measurements of the metallicity of the interstellar medium in other galaxies with a stellar mass, M_{\star} , of $\leq 10^9~M_{\odot}$ at $z\approx 2$ to 3 (20, 21) but consistent within 2σ with the CGM metallicity

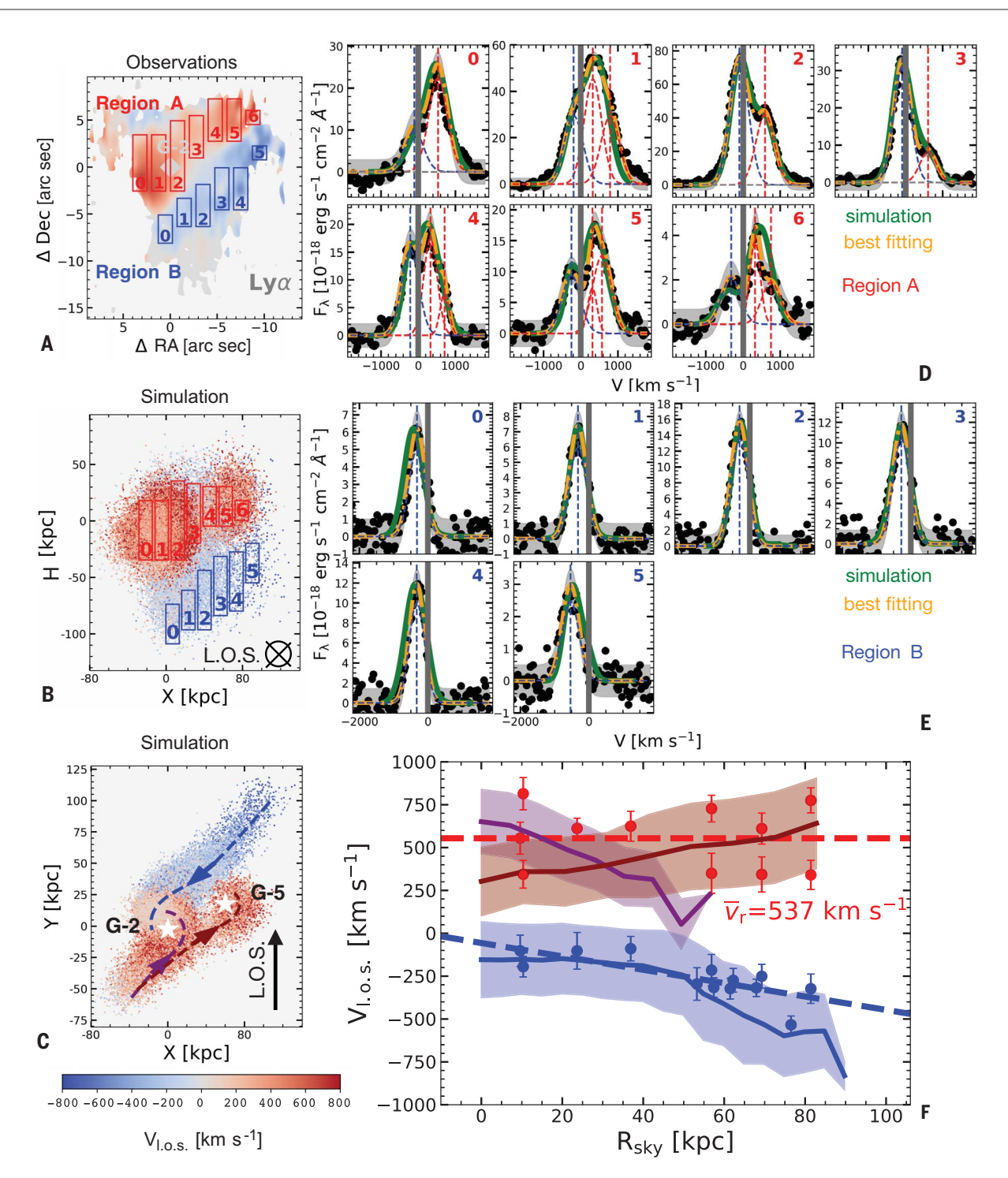


Fig. 4. Interpretation as an inspiraling stream. (**A**) Same as Fig. 1D, except regions A and B are divided into subregions indicated by the boxes, within which the spectra in (D) and (E) were extracted. (**B**) Same as (A), but for our simulation of the inspiraling streams model (15). The line of sight (L.O.S.) is along the y axis. (**C**) Projection of our model on the x–y plane. The two white stars mark the positions of G-2 and G-5. Three main inspiraling streams are shown with dashed lines, with arrows indicating flow directions. Two streams are around G-2, and the third stream is around G-5. Other projections of this model are shown in fig. S9. (**D** and **E**) Observed 1D spectra extracted from the regions shown in (A). The orange lines include multiple Gaussians, with each individual component shown as dashed lines, as in Fig. 2. Black dots represent the data, and the gray shaded region indicates the 1σ scatter. The green lines are the simulated spectra

extracted from the regions shown in (B). The data and the simulation are consistent. (**F**) Projected line-of-sight velocity profile of the observations (dots) obtained from the red and blue components of the spectra in (D) and (E). R_{sky} is the projected distance from each region to G-2 on the plane of the sky. The 11 red points correspond to the 11 redshifted Gaussians shown in (D), and the 13 blue points correspond to the 13 blueshifted Gaussians shown in (D) and (E). Error bars are 1σ . The dashed lines are linear models fitted to the data points. The solid lines with shaded areas are our simulated velocity profiles, with colors corresponding to the streams in (C). The shaded areas denote the 1σ scatter. The red components have a roughly constant velocity profile, whereas the absolute values of the blue components have an increasing profile. $\overline{\nu_r}$ is the mean of the observed redshifted velocities.

of some galaxies at $z\approx 0$ (22). Previous studies have found that metal-enriched gas, traced by C IV absorption toward background sources, is distributed within ≈ 125 kpc around galaxies at z=2 to 3 (23). Other studies have shown that CGM metallicity could be higher than Z_{\odot} at z=1 (24). Our measurements show that the CGM in MAMMOTH-1 has been enriched to between 0.1 and 1.0 Z_{\odot} on ≈ 100 -kpc scales.

Interpretation of the kinematics

We investigated whether the observed kinematics could be produced by an active galactic nucleus (AGN) outflow (see supplementary text in the supplementary materials). We find that they cannot, for two reasons: First, we expect any outflow to decelerate as it propagates into the CGM, as a result of energy loss (25-27). Instead, the observed line-of-sight velocity profile (Fig. 4F) shows that the redshifted velocity is roughly constant and that the absolute value of the blueshifted velocity increases with increasing distance from G-2. Secondly, if the kinematics was due to an AGN outflow, the observations would require an implausibly high coupling efficiency between the outflow power and the AGN luminosity (supplementary text) that is almost one order of magnitude greater than that found by previous observations or simulations (fig. S13).

Alternatively, the gas metallicity, spatial distribution, and kinematics could be due to metalenriched inspiraling streams. Gas in the CGM could have been enriched and expelled by previous outflows, from the AGN or starbursts in other galaxies. Cosmological simulations predict that inspiraling cool streams allow accreting galaxies to gain high angular momentum (4, 28). In cosmological simulations (29), ~46% of halos with masses $M_{\rm h} \ge 10^{13}\,M_{\odot}$ at z=2 have inspiraling streams that are metal-enriched on CGM scales (15). Those simulations predicted that, in addition to pristine gas accretion, accretion of recycled, metal-enriched gas could be a common process.

Motivated by those simulations, we constructed a simple kinematic model of metalenriched inspiraling streams to interpret our observations (*15*). The model consists of three inspiraling streams: two that surround G-2 and a third that surrounds G-5. The geometry of the model is shown in Fig. 4C. Comparing this model to the data, we find that both the simulated velocity map (Fig. 4B) and line profiles (Fig. 4, D and E) are consistent with the observations. The reduced χ^2 between the simulated and observed spectra is ~0.9. The kinematics is also reproduced by the model (Fig. 4F), within the 1 σ scatter.

Implications for gas accretion

Cosmological simulations have also shown that recycled inflows can provide gas accretion at $z \sim 0$ (8, 9). Other simulations (7) have shown

that, at z=2, the fraction of stellar mass contributed by recycled gas is 40% in a $10^{12.8}\,M_\odot$ halo. Our interpretation of the MAMMOTH-1 observations is consistent with the latter scenario (7).

We calculate that the streams provide a mass inflow rate $\dot{M}_{\rm in}=703^{+101}_{-78}M_{\odot}~{
m year}^{-1}$ (15), which is higher than the SFR of G-2 (81 \pm 18 M_{\odot} year⁻¹) derived from its far-infrared emission (15). We suggest that this indicates a link between the accretion rate of the recycled gas inflow and the SFR of G-2 (15). The observed line-of-sight velocity profile (Fig. 4F) is consistent with cool gas undergoing deceleration as it falls into the dark matter halo, as predicted by semianalytic models of cool CGM gas (30, 31). In those semianalytic models, the deceleration is interpreted as a consequence of drag forces exerted by the hot coronal gas on the cool gas stream. Because MAMMOTH-1 resides in the peak of overdensity that is also a galaxy group, the diffuse metal-enriched gas could also arise from galaxy interactions, such as tidal stripping. We estimate that this scenario is negligible on the CGM scale (supplementary text). A Hubble Space Telescope image of MAMMOTH-1 (Fig. 1K) shows no evidence of tidal stripping on large scales.

Our spectroscopic observations show that the group of galaxies within MAMMOTH-1 has a redshift gradient qualitatively consistent with that of the CGM (Fig. 1D and table S3). This indicates that the large-scale orbital angular momentum of the galaxy group aligns with the CGM angular momentum. Any satellite galaxies moving around G-2 could impart angular momentum to the enriched cool CGM gas, which would then flow back to the galaxy in an inspiraling stream (fig. S8A). The CGM gas flow would then induce a shock, facilitating gas cooling through line emission. From the estimated inflow rate of the recycled gas, the recycled inflow could sustain star formation in G-2 at this redshift.

REFERENCES AND NOTES

- J. Tumlinson, M. S. Peeples, J. K. Werk, Annu. Rev. Astron. Astrophys. 55, 389–432 (2017).
- D. Kereš, N. Katz, D. H. Weinberg, R. Davé, Mon. Not. R. Astron. Soc. 363, 2–28 (2005).
- J. Stern, D. Fielding, C.-A. Faucher-Giguère, E. Quataert, Mon. Not. R. Astron. Soc. 492, 6042–6058 (2020).
- 4. K. R. Stewart et al., Astrophys. J. **843**, 47 (2017).
- J. Suresh, D. Nelson, S. Genel, K. H. R. Rubin, L. Hernquist, Mon. Not. R. Astron. Soc. 483, 4040–4059 (2019).
- 6. N. Lehner et al., Astrophys. J. 887, 5 (2019).
- D. Anglés-Alcázar et al., Mon. Not. R. Astron. Soc. 470, 4698–4719 (2017).
- R. J. J. Grand et al., Mon. Not. R. Astron. Soc. 490, 4786–4803 (2019).
- B. D. Oppenheimer et al., Mon. Not. R. Astron. Soc. 406, 2325–2338 (2010).
- 10. R. Brennan et al., Astrophys. J. 860, 14 (2018).
- J. X. Prochaska, M. W. Lau, J. F. Hennawi, Astrophys. J. 796, 140 (2014).
- 12. Z. Cai et al., Astrophys. J. 837, 71 (2017).
- 13. F. Arrigoni Battaia et al., Astron. Astrophys. **620**, A202 (2018).
- B. H. C. Emonts, Z. Cai, J. X. Prochaska, Q. Li, M. D. Lehnert, Astrophys. J. 887, 86 (2019).

- Materials and methods are available as supplementary materials.
- Q. Li et al., Astrophys. J. 922, 236 (2021).
- Y. Yang, A. Zabludoff, K. Jahnke, R. Davé, Astrophys. J. 793, 114 (2014).
- 18. F. Arrigoni Battaia et al., Astrophys. J. 804, 26 (2015).
- M. G. Allen, B. A. Groves, M. A. Dopita, R. S. Sutherland, L. J. Kewley, Astrophys. J. Suppl. Ser. 178, 20–55 (2008).
- 20. C. C. Steidel et al., Astrophys. J. 795, 165 (2014).
- 21. J. Tumlinson et al., Science 334, 948-952 (2011).
- 22. C. B. Wotta et al., Astrophys. J. 872, 81 (2019).
- 23. C. C. Steidel et al., Astrophys. J. 717, 289-322 (2010).
- N. Lehner, J. M. O'Meara, J. C. Howk, J. X. Prochaska, M. Fumagalli, Astrophys. J. 833, 283 (2016).
- 25. A. C. Fabian, Annu. Rev. Astron. Astrophys. **50**, 455–489 (2012).
- A. J. Richings, C.-A. Faucher-Giguère, Mon. Not. R. Astron. Soc. 478, 3100–3119 (2018).
- 27. C. Circosta et al., Astron. Astrophys. **620**, A82 (2018).
- 28. K. R. Stewart et al., Astrophys. J. 738, 39 (2011).
- 29. D. Nelson et al., Comput. Astrophys. Cosmol. 6, 2 (2019).
- T.-W. Lan, H. Mo, Mon. Not. R. Astron. Soc. 486, 608–622 (2019).
- 31. A. Afruni, F. Fraternali, G. Pezzulli, *Astron. Astrophys.* **625**, Al1 (2019).

ACKNOWLEDGMENTS

We thank the anonymous referees for insightful comments that substantially improved the manuscript, Z.C. and S.Z. thank S. Cantalupo, H.-W. Chen, M. Gronke, K. Kakiichi, C. Martin, M. Matuszewski, V. Springel, Y. Su, and H. Zhou for useful discussions. Z.C. and S.Z. also thank J. Zou and B. Wang for proofreading the manuscript. Funding: Z.C., S.Z., and Y.W. are supported by the National Key R&D Program of China (grant 2018YFA0404503), the National Science Foundation of China (grant 12073014). and Tsinghua University Initiative Scientific Research Program (grants 20223080023 and 20221080006). D.X. and S.W. are supported by the Tsinghua University Initiative Scientific Research Program (grant 2019Z07L02017). R.S. acknowledges support from Grantsin-Aid for Scientific Research (KAKENHI; 19K14766) through the Japan Society for the Promotion of Science (JSPS), 7.7, is supported by NSF grant AST-2007499. A.Z. acknowledges funding from NSF grant AAG-1715609. Author contributions: Z.C. conceived of the project. S.Z. and Z.C. led the data reduction, analysis, and manuscript writing. Z.C., R.S., J.X.P., X.F., and Q.L. led the telescope proposals, with Z.C. as the principal investigator of most of the proposals. R.S. contributed to the observations and data reduction of the MORICS data, D.X., F.A.B., and R.C. contributed to the theoretical interpretation. L.D., J.W., and Y.A contributed the analysis of the x-ray observations. R.C., Z.Z., A.Z., E.G.G.-M., M.L., Y.L., X.M., S.W., R.W., Y.W., and F.Y. contributed to the scientific interpretation and writing of the manuscript. All authors discussed the results and commented on the manuscript. Competing interests: The authors declare that they have no competing interests. Data and materials availability: The observational data are available in the Keck/KCWI archive (https://koa.ipac.caltech.edu/cgi-bin/KOA/nph-KOAlogin) under program ID N052; the ALMA and VLA archive (https:// data.nrao.edu/portal/#/) under project codes 17A-174 and 2018.1.00859.S: the HST archive (https://mast.stsci.edu/search/ ui/#/hst) under proposal ID 14760; the Chandra data archive (https://cda.harvard.edu/chaser/) under observation ID 20357; and the Subaru archive (https://smoka.nao.ac.jp/fssearch.jsp) by selecting MOIRCS under "Instruments" and then entering "MAMMOTH-1" as the object name. The results of our spectral fitting are provided in tables S1 and S2, our measured redshifts in table S3. and the parameters of our streams model in table S4. License information: Copyright © 2023 the authors, some rights reserved; exclusive licensee American Association for the Advancement of Science. No claim to original US government works. https://www. science.org/about/science-licenses-journal-article-reuse

SUPPLEMENTARY MATERIALS

science.org/doi/10.1126/science.abj9192 Materials and Methods Supplementary Text Figs. S1 to S13 Tables S1 to S4 References (32–78)

Submitted 18 June 2021; accepted 31 March 2023 10.1126/science.abj9192



Inspiraling streams of enriched gas observed around a massive galaxy 11 billion years ago

Shiwu Zhang, Zheng Cai, Dandan Xu, Rhythm Shimakawa, Fabrizio Arrigoni Battaia, Jason Xavier Prochaska, Renyue Cen, Zheng Zheng, Yunjing Wu, Qiong Li, Liming Dou, Jianfeng Wu, Ann Zabludoff, Xiaohui Fan, Yanli Ai, Emmet Gabriel Golden-Marx, Miao Li, Youjun Lu, Xiangcheng Ma, Sen Wang, Ran Wang, and Feng Yuan

Science, 380 (6644), .

DOI: 10.1126/science.abj9192

Editor's summary

Galaxies accrete gas from the surrounding intergalactic medium and then turn this gas into stars. Feedback processes such as supernova explosions enrich the gas with elements heavier than helium and can impart enough momentum to eject some gas out of the galaxy. S. Zhang et al. observed the intergalactic medium around a massive galaxy at redshift 2.3. In addition to emission lines caused by hydrogen and helium, they observed lines for carbon, indicating that the gas has been enriched with heavier elements. The kinematics are consistent with streams of gas spiraling toward the massive galaxy. The authors propose that the enriched gas has been recycled from an earlier period of star formation. —Keith T. Smith

View the article online

https://www.science.org/doi/10.1126/science.abj9192

Permissions

https://www.science.org/help/reprints-and-permissions

Use of this article is subject to the Terms of service